XLI CILAMCE
XLI Ibero-Latin American Congress on Computational Methods in Engineering
16-19 November, 2020 FOZ DO IGUAÇU PARANÁ - BRAZIL

Application of peridynamics in the simulation of acoustic emission in quasi-brittle materials

Pricila Cottica[1], Leandro Friedrich[1], Ederli Marangon[1], Ignacio Iturrioz[2]

[1]*Graduate Program in Engineering, Federal University of Pampa*
Av. Tiaraju 810, CEP 97546-550, RS/Alegrete, Brazil.
pricilacottica.aluno@unipampa.edu.br, leandrofriedrich@unipampa.edu.br, ederlimarangon@unipampa.edu.br
[2]*Mechanical Post-Graduate Program, Federal University of Rio Grande do Sul*
Sarmento Leite 425, CEP 90050-170, RS/Porto Alegre, Brazil.
ignacio.iturrioz@ufrgs.br

Abstract. The acoustic emission (AE) technique consists in capturing the internal mechanical waves produced by materials due to changes such as chemical reactions, cracks, dislocations, among others, that propagates for the surfaces of the structure and are captured by sensors distributed on these surfaces generating the AE events. This methodology has been used to monitor the damage of real structures, allowing predicting when an event of greater magnitude could mean the imminence of a total or partial collapse. In addition, the technique of acoustic emission allows extracting information from structures formed by quasi-brittle materials where the succession of instabilities has a pattern of behavior can be established. The interpretation of acoustic emission tests is not trivial and the simulation of this type of test can complement the information about the experimental test performed. Aligned with the topic mentioned here, in the present work, an acoustic emission test on concrete specimens is simulated. To perform the numerical simulations, a version of the discrete element method called peridynamics was used. The results show that the peridynamic theory is a powerful tool and can be used to help in the planning and interpretation of experimental results from the monitoring of structures.

Keywords: peridynamics, acoustic emission, quasi-brittle materials.

1 Introduction

The acoustic emission technique is based on the study of elastic tension waves released by some disturbance in the material, such as the appearance of cracks, dislocations, among others. These waves are registered by a transducer fixed to the surface of the structure that converts the movements resulting from the damage into an electrical signal, in the form of a discrete wave, for further analysis, Shahidan [1]. The interpretation of acoustic emission tests is not trivial and the simulation of this type of test can complement the information about the experimental test performed. Peridynamics (PD) is one of the methods that has shown great applicability in solving engineering problems in general. The theory is a particular formulation of the discrete element method, DEM, developed by Silling, [2]. The equations that govern peridynamics are integral-differential and do not contain spatial derivations, this characteristic makes the theory very interesting for analyzing and monitoring problems such as the initiation and propagation of cracks, Rädel [3].

In this work, an acoustic emission test of a concrete specimen subjected to four-point bending through peridynamics is simulated. The model material is calibrated by comparing the experimental Force x Deflection curves of concrete specimens in four-point bending test. From the acoustic emission signal register, the spatial distribution of events, acoustic emission energy as well as the predominant form of damage during the material failure process will be analyzed.

2 Peridynamics

For Kilic and Madenci [4], displacement derivatives do not appear in the peridynamic equations, this allows them to be valid anywhere, with or without displacement discontinuities. In Silling [2], the peridynamic equation of motion is described in a reference configuration of the position x and time t, given as eq. (1):

$$\rho\ddot{u} = \int_{H_x} f(x, x', u(x,t), u(x',t))dV_{x'} + b(x,t) \tag{1}$$

where ρ is the density, $\ddot{u}$ is the acceleration vector, b the body forces, that is, the external forces, H_x it is called the point x family that determines the other material points that interact with point x, see Fig. 1a. For a linear elastic isotropic solid [4], for example, it can be expressed as eq. (2):

$$f(u' - u, x' - x) = cs\frac{y' - y}{|y' - y|} \tag{2}$$

where $y = x + u$ is the position of the material point in the deformed configuration and c the bond constant, for 3D case, $c = 12E / \pi\delta_0^4$ where E is the elastic modulus of material and δ_0 is called a horizon that defines the region of interaction between material points, Fig. 1a. In the eq. (2), s is the bond stretch expressed on the following form,

$$s = \frac{|y' - y| - |x' - x|}{|x' - x|} . \tag{3}$$

To model the quasi-brittle material behavior, the bilinear law proposed by Cabral *et al*. [5] is used to replace the classic uniaxial law of PD, Fig 1b. It is important to mention in this formulation the horizon (δ_0) is defined as a parameter of the material and not of the model (δ'), which can be adopted as the convenience observing the increase in computational time when this value increases. Thus the bilinear law makes an equivalence between the energies with the material and computational horizon, making the law more flexible and allowing to change the global behavior of the material. For more information on the bilinear law and the calibration of the parameters, see Cabral *et al*. [5].

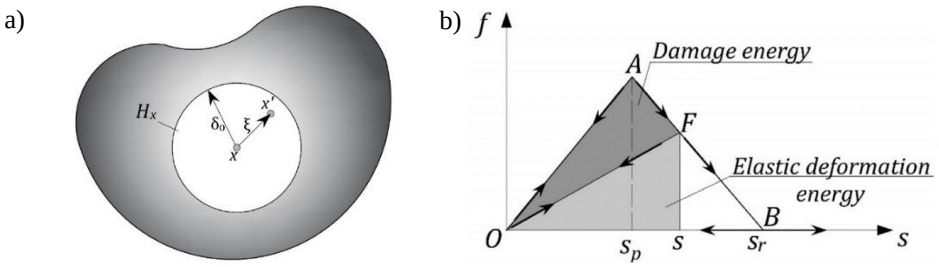

Figure 1. a) Proposed law and its relation with the involved energies in the loading process, Silling and Askari [6], b) Bilinear law representation, Cabral *et al.* [5]

The critical condition is reached when s is equal to or greater than s_r Fig. 1b, equal to:

$$s_r = K_r s_p, \quad K_r = s_0 d_0 / s_p d' \tag{4}$$

where K_r makes the relationship between the maximum linear stretch (s_p) and the critical stretch in the bilinear law (s_r), see Fig. 1b. s_p can be estimated, when experimental results are available, as the strain in which the structure loses its linearity. In eq. (4) s_0 is the critical stretch of the bond. This parameter is the same in the classic uniaxial law, and for 3D case, can be defined in terms of the macroscopic fracture energy G_f:

$$s_0 = \sqrt{5G_f / 6E\delta_o} . \tag{5}$$

In the PD model to better represent the material's heterogeneity as Friedrich et al. [7] showed, G_f is assumed

to have a Weibull probability distribution given by:

$$p(G_f) = 1 - \exp[-(G_f / b)^g] \quad (6)$$

being β and γ the scale and shape parameters, respectively. Such parameters can be computed through the coefficient of variation CV_{Gf} defined as the ratio between the standard deviation s_{Gf} and the mean value of the specific fracture energy G_f. However, a spatial correlation function for G_f needs to be defined. The correlation lengths *Lcx*, *Lcy*, *Lcz* along the three directions *x*, *y* and *z*, respectively. Details may be found in Puglia *et al*. [8].

3 Acoustic emission monitoring

Aggelis [9], describes that the acoustic emission is studied in relation to the evolution of the damage under dynamic load or in relation to the crack propagation rate. It is expected is that the number of signals recorded during loading can be correlated with the actual number of active cracks within the material and thus obtain a real diagnosis of the structure's conditions. Shahidan [1] describes that the parameters used to interpret the data obtained through the acoustic emission are fundamental for a correct diagnosis. The parameters are established from a typical event, as shown in Fig. 2, characterized by the first and last peak to exceed the Threshold (level of amplitude values from which the signal is considered an Acoustic Emission event) and by the Peak amplitude which is the biggest signal of the event.

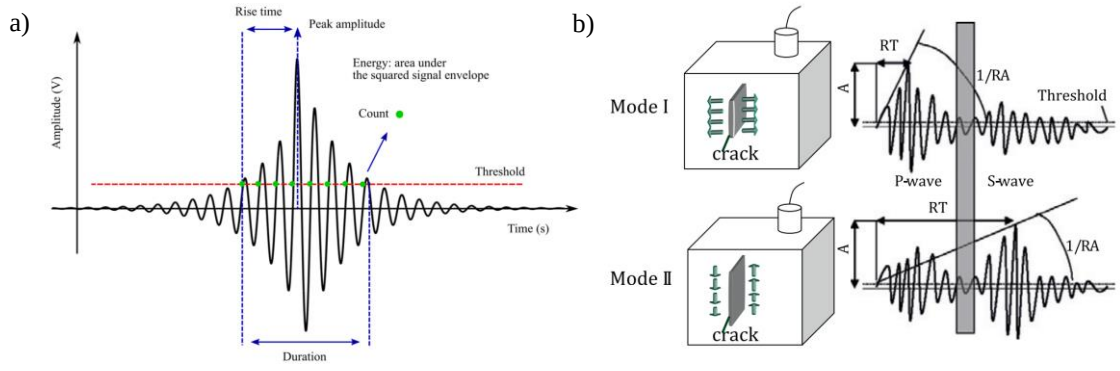

Figure 2. a) Common acoustic emission event features, Shateri *et al*. [10], b) Cracking mode due to AE signal Aggelis *et al.* [9]

According to Grosse and Ohtsu [11], the main parameters used for the interpretation of AE events are: the Rise Time (RT) which refers to the time observed between the first signal value that passes through the Threshold, until the time of the maximum amplitude of the event; the Average Frequency (AF), usually obtained in KHz, is defined by the ratio of two other parameters - Counts (number of times the acoustic emission signal exceeds the threshold), and Duration (time the signal remains above the threshold) ; and Rise Angle (RA) value determined by the rise time (RT) divided by the amplitude. The RA x AF relationship allows us to identify the different waveforms and the different fracture mechanisms that occur during the evolution of the damage to the structure, classified as Mode I (tensile cracks) and Mode II (shear cracks). Example of waveforms and crack Modes are shown in Fig. 2b. In addition parameters such as amplitude, signal strength and energy can be analyzed to determine and characterize the level of damage.

4 Peridynamic model description

To illustrate the application previously mentioned, we used an experimental four-point bending tests on concrete beam for material validation, Marangon [12]. The specimen size was 100x100x400 mm with a span of 300 mm. The concentrated loads were distributed at each 1/3 of the span length, in accordance with the NBR NM 55 standard [13]. Three specimens were subjected to the experimental career. The results in terms of the Load x

Displacement curves and the fracture configuration will be used to evaluate the PD results. In Fig. 3, geometric properties, boundary conditions, loads (prescribed displacement) and the spatial distribution of virtual AE sensors are showed. The simulate accelerometers that register the motion capturing the signal with 2 MHz sampling rate. The PD model consisted of 80 × 20 × 20 material points. The material properties, model and constitutive law parameters are indicated in Tab. 1. To apply the random field, a coefficient of variation of 80% was defined, and a correlation length equal in all directions and equivalent to 3 times of the maximum aggregate size (d_{max}). As in the experimental case, three samples were simulated in the PD from the change of the generated random field Friedrich *et al*. [7].

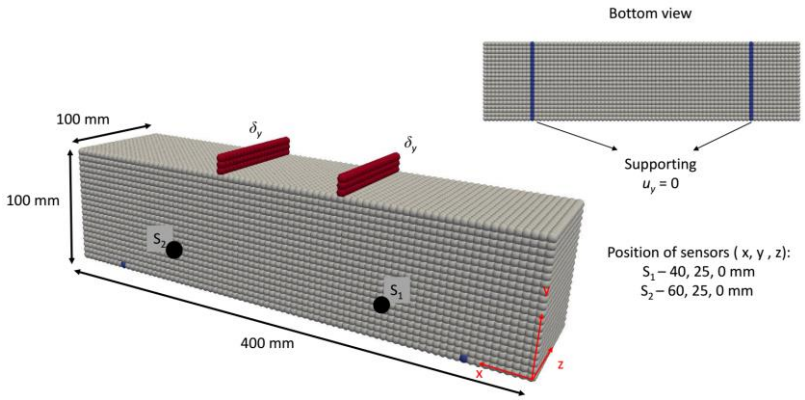

Figure 3. Beam dimensions, boundary condition, applied loading and sensors position

Table 1. Mechanical properties and model parameters

E [MPa]	ν	ρ [kg/m^3]	G_f [N/m]	$d_{\max}$ [m]	$CV(G_f)$ [%]	dx [m]	s_p	K_r	δ' [m]	δ_0 [m]
35.6	0.25	2400	80	0.0095	80	0.005	1.1e^{-4}	10	3.015dx	0.028

5 Results and discussion

Figure 4a shows the comparison between the Load x Displacement curves of the tests in lab and PD simulations. The results of the PD adhere very well to the experimental curves of the cementitious material.

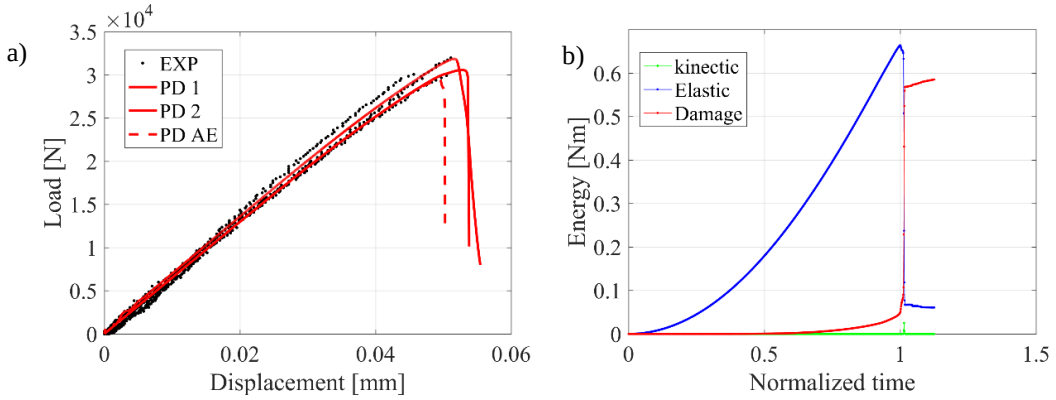

Figure 4. a) Comparison of PD and experimental results, b) energy balance of the PD_AE case

The energy balance during the process is presented in Fig. 4b. It may be seen that the elastic strain energy increases monotonically until the peak load is reached (before it the kinetic energy remains low) and the unstable

propagation begins. The damage distribution starts at the bottom face of the beam (Fig. 5b) and is the source for the first AE hits. Near the peak load, the damage growth through the central region of the sample until it separates the body.

Figure 5 shows the comparison between the fracture patterns obtained by the PD and the experimental results. To better visualize the damaged regions, only material points with a non-zero damage index are presented. The tortuosities recorded in the experiment are also captured by the PD indicating that the parameters used to define the random field are satisfactory.

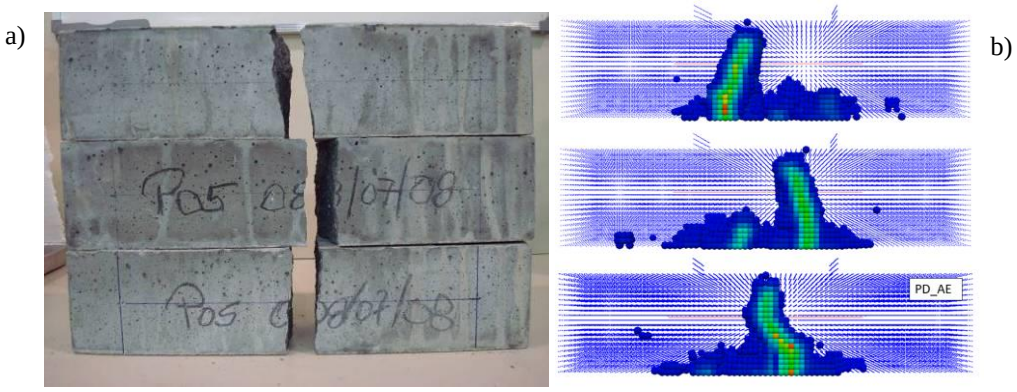

Figure 5. Fracture configuration a) experimental, Marangon, [12], b) PD simulations

Results of the acoustic monitoring concern the total activity and the qualitative features of the waveforms. Figure 6 shows the accumulated AE signals (hits) and the acoustic emission energy (out of scale) by the sensor 1 and 2 in the normalized time (time/time of peak load) of the sample called PD_AE. For both of sensors the number of hits is built gradually until the moment of final failure where the maximum hit rate is exhibited. In sensor 1 it is possible to see clearly that there are 3 distinct regions of change in the internal damage rate of the material. Note that between points 1-2 several events are recorded, but they do not cause significant damage as can be seen from the load curve that remains unchanged. However, in region 2-3 a large number of events are recorded and the rate of internal damage to the material increases as shown by the AE energy. In addition, the structure loses its linear behavior and the damage begins to affect the initial stiffness of the material. Finally, in the last region the energy increases again in the final test phase until the sample collapses.

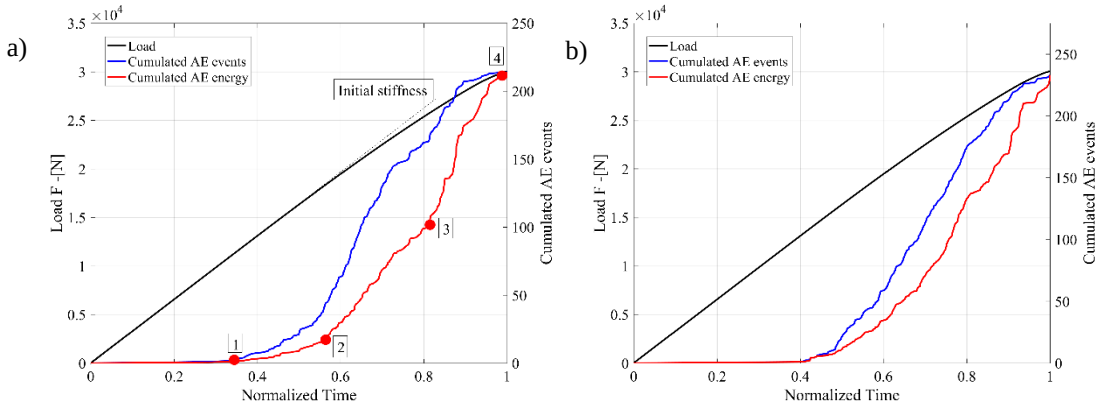

Figure 6. The accumulated AE signals (hits) and the acoustic emission energy by a) S_1 and, b) S_2

Figure 7 shows the RA and AF of the signals received by the S_1 and S_2 sensor. A result to highlight is the maximum frequencies captured in the model, between 80 -150 kHz, typical frequencies obtained in experimental tests of acoustic emission on concrete specimens [1, 9]. In fact, it is not possible to notice a great difference between the behaviors registered in each sensor, but in a visual analysis of the signal, a change in the waveforms is noticed

as the source is closer to one sensor than the other. However, this does not completely modify the RA and AF parameters. On the contrary, experimental results by Aggelis [9, 14] analyzing this problem show that the differences measured by two sensors in different distances are dependent on the testing conditions, geometry restrictions, material or damage-induced inhomogeneity and the distance between the cracks and the sensors. PD is less affected by many of the problems mentioned and can help complement studies in this field.

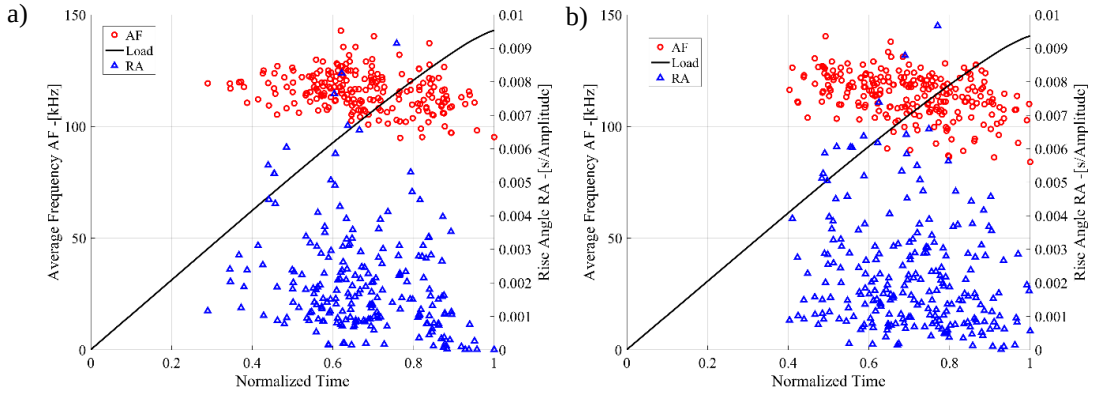

Figure 7. RA and AF paramters vs normalized time for a) S_1 and, b) S_2

The failure occurred due to crack propagation in the bottom face of the beam, provoked principally by tensile stresses. The fracture mode was analyzed by means of the relationship between RA and AF values estimated for each sensor, as shown in Figure 8a. Considering that a decrease in the AFs by approaching the peak load is obtained, and that the RA values are all lower than 0.01 s/A, a dominant presence of tensile cracks (Mode I) characterizes the damage evolution up to the final collapse.

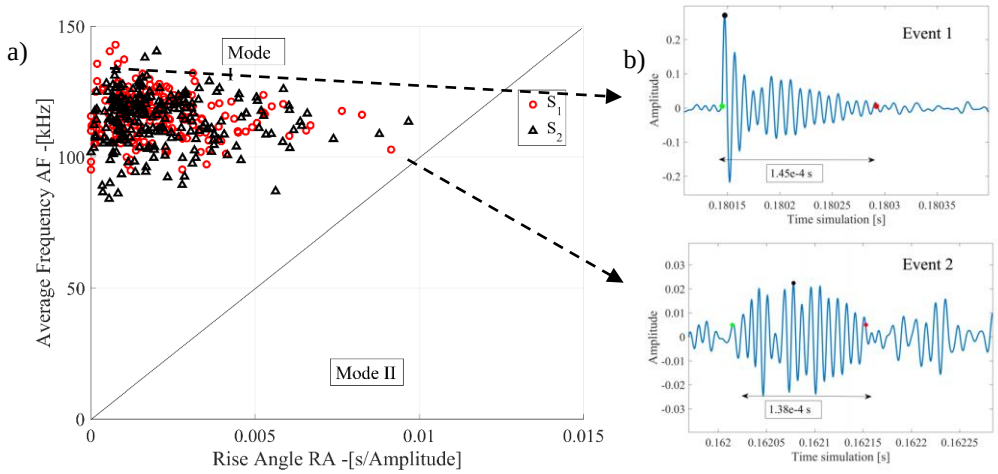

Figure 8. a) Classification type of cracking (RA x AF) and, b) Typical Events registered

As expected, the normal stresses in the bending exhibit a positive maximum at the mid span where the specimens actually broke as shown by the experimental and numerical result (Fig. 5). This happens due to the weak tensile strength of cementitious material, in the experimental samples the average value of maximum tension strength is 9.15 MPa. Therefore, the crack at the center of the specimen can be considered quite close to pure tensile mode, as registered in the Fig. 8a. However, in a visual analysis we can find some events with waveforms very similar to Mode II (Event 2) and are located close to the dividing line between the failure modes as shown in Fig. 8b. A typical Mode I event (Event 1) recorded by the PD simulation is also presented, where the green, black and red points are the start, peak and end times of the events.

6 Conclusions

In the present work, we evaluated the application of peridynamic theory in the simulation of an acoustic emission test on a beam in a four-point bending test. In addition, through the bilinear law we were able to represent the mechanical behavior of the concrete material used to calibrate the model comparing the experimental Load x Displacement curves. The temporal distribution of the events was evaluated and some parameters of acoustic emission were calculated to diagnose the evolution of the damage in the material. The results show that the peridynamic theory is a powerful tool and can be used to help in the planning and interpretation of experimental results from the monitoring of structures.

Acknowledgements. The authors wish to thank the National Council for Scientific and Technological Development (CNPq - Brazil) and Coordination for the Improvement of Higher Education Personnel (CAPES - Brazil) for funding this research.

Authorship statement. The authors hereby confirm that they are the sole liable persons responsible for the authorship of this work, and that all material that has been herein included as part of the present paper is either the property (and authorship) of the authors, or has the permission of the owners to be included here.

References

[1] S. Shahidan, *et al*, "Damage classification in reinforced concrete beam by acoustic emission signal analysis". *Construction and Building Materials*, v. 45, p. 78-86, 2013.
[2] S.A Silling, "Reformulation of elasticity theory for discontinuities and long-range forces". *Journal of the Mechanics and Physics of Solids*, vol. 48, pp. 175–209, 2000.
[3] M. Rädel, *et al*., "Peridynamics: Convergence & Influence of Probabilistic Material Distribution on Crack Initiation". 6th *ECCOMAS Themat.* Conf. Mech. Response Compos, 2017.
[4] B. Kilic and E. Madenci, "Predição de trajetórias de trincas em uma placa de vidro temperada usando a teoria peridinâmica". *Jornal internacional de fratura* , v. 156, n. 2, pág. 165-177, 2009.
[5] N. R. Cabral, M. A. Invaldi, R. B. D'Ambra, I. Iturrioz, An alternative bilinear peridynamic model to simulate the damage process in quasi-brittle materials, *Engineering Fracture Mechanics*, V. 216, 2019.
[6] S.A. Silling, and E. Askari, "A meshfree method based on the peridynamic model of solid mechanics". *Computers & Structures*, vol. 83, pp. 1526–35, 2005.
[7] L. Friedrich, *et al*., "Random field generation of the material properties in a peridynamic model", In: *25th ABCM International Congress of Mechanical Engineering*, Uberlândia, MG, Brazil, 2019.
[8] V. B. Puglia, *et al*., "Random field generation of the material properties in the lattice discrete element method". *The Journal of Strain Analysis for Engineering Design*, vol. 54, pp. 236–246, 2019.
[9] D. G. Aggelis, *et al*., "Effect of wave distortion on acoustic emission characterization of cementitious materials". *Construction and Building Materials*, v. 35, p. 183-190, 2012.
[10] M. Shateri, *et al*., "On acoustic emission for damage detection and failure prediction in fiber reinforced polymer rods using pattern recognition analysis". *Smart Materials and Structures*, v. 26, n. 6, p. 065023, 2017.
[11] C. U. Grosse and M. Ohtsu., "Acoustic Emission Testing". Springer Berlin Heidelberg, 2008.
[12] E. Marangon, "Desenvolvimento e caracterização de concretos autoadensáveis reforçados com fibras de aço". Dissertação de Mestrado-Universidade Federal do Rio de Janeiro, 2006.
[13] NBR NM 55. Concreto – Determinação da resistência à Tração na Flexão de Corpos-de-prova Prismáticos, 1996.
[14] D. G. Aggelis, "Classification of cracking mode in concrete by acoustic emission parameters". *Mechanics Research Communications*, v. 38, n. 3, p. 153-157, 2011.